RESEARCH ARTICLE | JUNE 02 2026

Infrared thermography measurements of an unsteady laminar separation bubble on a static and pitching airfoil

L. Riccobene ; M. Poletti ; R. Tomasello ; A. Zanotti

Physics of Fluids 38, 064108 (2026)
https://doi.org/10.1063/5.0323230

Physics of Fluids ARTICLE pubs.aip.org/aip/pof

Infrared thermography measurements of an unsteady laminar separation bubble on a static and pitching airfoil

Cite as: Phys. Fluids **38**, 064108 (2026); doi: 10.1063/5.0323230
Submitted: 16 January 2026 · Accepted: 19 May 2026 ·
Published Online: 2 June 2026

View Online Export Citation CrossMark

L. Riccobene,[a] M. Poletti, R. Tomasello, and A. Zanotti

AFFILIATIONS

Politecnico di Milano, Dipartimento di Scienze e Tecnologie Aerospaziali, via La Masa 34, 20156 Milan, Italy

[a]Author to whom correspondence should be addressed: luca.riccobene@polimi.it

ABSTRACT

The present work describes infrared thermography (IRT) measurements conducted on a National Advisory Committee for Aeronautics (NACA) 0018 airfoil model aimed at characterizing a laminar separation bubble (LSB) at low Reynolds numbers under steady and sinusoidal pitching conditions. In steady flow conditions, the accuracy of best practices described in the literature for surface temperature measurements applied to the quantitative assessment of LSB characteristic points (separation, transition, and reattachment) was investigated through a comparative study between IRT measurements and surface flow visualizations. In unsteady flow conditions, the differential infrared thermography (DIT) technique enabled the evaluation of the effects of reduced frequency, oscillation amplitude, and Reynolds number on the behavior of the LSB characteristic point positions along the pitching cycle, with particular emphasis on the reattachment point. The results show a pronounced hysteresis in the characteristic point locations, especially during the upstroke motion, which increases approximately linearly with both pitch rate and oscillation amplitude, while increasing the Reynolds number promotes an upstream shift of the LSB characteristic points. Overall, the present work demonstrates the effectiveness of DIT as a high-resolution, non-intrusive technique for monitoring time-resolved LSB dynamics in unsteady aerodynamic applications.

NOMENCLATURE

Latin symbols

c	Chord length (meter)
C_p	Specific heat capacity ($\mathrm{J\,kg^{-1}\,K^{-1}}$)
f	Pitching frequency (Hz)
I	Thermal intensity (counts)
k	Reduced frequency, $k = \pi fc/U_\infty$
Re	Reynolds number
U_∞	Free-stream velocity ($\mathrm{m\,s^{-1}}$)
X/c	Non-dimensionalized chordwise coordinate (–)

Greek symbols

α	Angle of attack (deg)
$\bar{\alpha}$	Mean angle of attack (deg)
$\hat{\alpha}$	Pitching amplitude (deg)
λ	Thermal conductivity ($\mathrm{W\,m^{-1}\,K^{-1}}$)

I. INTRODUCTION

The transition from a laminar to a turbulent boundary layer (BL) is of critical importance regarding the aerodynamic performance of an aircraft. Indeed, a laminar flow that extends for as much chord length as possible enables the reduction of viscous drag and therefore reduces fuel or power consumption. To evaluate these potential improvements in aerodynamic efficiency or savings in fuel costs, the location of boundary layer transition should be accurately predicted.[1] The determination of the transition position is particularly challenging in wind tunnel experiments, as differences in the boundary layer transition location occur over a scaled model, which do not scale with the size of the model.[2]

Infrared thermography (IRT)[3] is one of the most efficient methods to assess the boundary layer transition position, exploiting the different convective heat flux levels between laminar and turbulent boundary layers.[4] Indeed, the infrared energy radiating from the object under investigation is detected by an infrared camera,

providing a map of the model surface temperature distribution. Each temperature level corresponds to a certain level of radiated energy and is represented in the image by a different gray scale level.[5,6] Compared to other measurement techniques, IRT presents many advantages as it is a non-intrusive and nondestructive technique that does not require particular surface coatings or direct contact of probes/instruments with the tested object. This latter feature is particularly preferable for the study of BL transition, for example, with respect to temperature sensitive paint (TSP), because of the sensitivity of the flow to environmental disturbances, particularly at low chord Reynolds numbers (*Re*), that could affect the boundary conditions of the flow near the wall.[7]

Differential infrared thermography (DIT) is an approach introduced by Raffel and Merz[8] specifically for the challenging task of unsteady BL transition measurements. The authors demonstrated that subtracting a reference image (or a temporal average) from the instantaneous thermal image dramatically enhances the contrast at the transition front, making the technique viable even in dynamic environments. Generally, as shown by Gardner *et al.*,[9] the differential processing of thermal images significantly enhances the signal-to-noise ratio (SNR), enabling precise and automated transition localization under both static and moderately dynamic conditions. To further refine the IRT tool, Wolf *et al.*[10] systematically optimized the DIT methodology, establishing best practices for reference image selection to maximize accuracy in highly dynamic environments, while also showing the capability of this technique for static measurements. The DIT technique was therefore applied to the detection of BL transition on pitching blade models.[10] Indeed, Raffel *et al.*[11] successfully demonstrated DIT's capability to track the rapid movement of the BL transition point across the blade surface during a full pitch cycle, correlating the transition location with changes in the instantaneous angle of attack. Later on, Gardner *et al.*[12] applied the IRT technique on a full-scale helicopter rotor, providing transition data in a highly three-dimensional and unsteady flow environment. The comprehensive review by Wolf *et al.*[13] summarized the advancements in the use of such techniques, confirming the maturity of IRT for transition measurements in aeronautical research.

On the other hand, the identification of BL transition on airfoils operating at low Reynolds numbers[14] and characterized by large thickness represents a quite challenging aspect in fluid dynamics. Indeed, for the present test cases, BL transition takes place over a laminar separation bubble (LSB).[14,15] A LSB is a three-dimensional aerodynamic feature consisting of a pocket of stagnant, recirculating flow. In a two-dimensional slice, as represented in Fig. 1, the LSB begins at the *laminar separation point* due to an adverse pressure gradient, then a laminar shear layer is created. Due to instability and disturbance

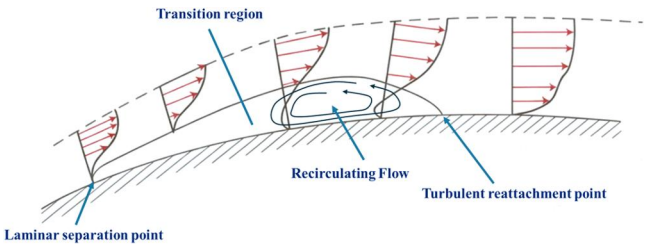

FIG. 1. Representation of a laminar separation bubble (LSB).

growth, the laminar shear layer transitions into a turbulent one at the *transition point*. Eventually, the turbulent shear layer reattaches to the surface at the *reattachment point* and an attached boundary layer is developed.

Infrared thermography could be considered among the most suitable experimental techniques for the investigation of such a challenging phenomenon. Early work of de Luca *et al.*[7] highlights the possibility of detecting the presence of laminar separation bubbles over an airfoil surface using the IRT technique. However, their work does not apply IRT to explicitly compute the locations of the points of interest for LSB position detection. Montelpare and Ricci[16] performed surface pressure and temperature measurements using IRT over an Eppler 387 airfoil at $Re = 100\,000$ and 200 000 for which transition occurs over an LSB. The authors noted that, since within the bubble the flow is almost stationary, the recirculation of air should be characterized by a drop in convective heat transfer. For a constant heat flux boundary condition, the surface temperature only depends on the convective heat transfer coefficient; therefore, applying the Reynolds analogy and considering convection as the main mechanism for heat transfer, it should be possible to identify the LSB as a region characterized by a local surface temperature increase along the chord. More recently, the study by Ricci *et al.*[17] investigated the influence of mechanical disturbances (e.g., periodic vibrations or flow perturbations) on the bubble's characteristics, specifically its length and location.

Transition to turbulence occurs in the separated shear layer, thus it is essential to correctly identify the points of separation and reattachment of the flow on the suction side of the airfoil. For these reasons, an accurate experimental evaluation of the characteristic transition points' positions related to the occurrence of an LSB represents an essential aspect for the characterization of the airfoil performance, as well as for validating and calibrating numerical prediction tools. Recent studies by Wynnychuk and Yarusevych[18] and Grille Guerra *et al.*[19] investigated systematically the positions of the three LSB key characteristic points on a stationary and pitching airfoil starting from the chordwise surface temperature/intensity distributions obtained from thermal images by combining the use of IRT with particle image velocimetry (PIV). In particular, Grille Guerra *et al.*[19] took advantage of IRT, PIV, and surface pressure measurements to characterize the flow over a modified National Advisory Committee for Aeronautics (NACA) 64_3618 at $Re = 200\,000$. This research focused on the time-resolved dynamics of the LSB, which significantly influences airfoil performance and dynamic stall inception, providing high-resolution data on how flow unsteadiness and the movement of the airfoil wall influence the LSB stability and size. Moreover, a comparison of the results obtained from classical IRT and DIT in steady conditions shows good agreement between the locations of the LSB characteristic points, with a discrepancy lower than 1% of the airfoil chord, providing proof of the applicability of DIT to detect LSB characteristics. On the other hand, Wynnychuk and Yarusevych[18] investigated the flow over a steady NACA 0018 airfoil at chord Reynolds numbers $Re = 80\,000$ and 120 000. In this work, a methodology for surface temperature-based diagnostics of LSBs was established through a comparative analysis coupling planar, two-component PIV data with surface temperature characteristics. Under convection-dominated surface cooling, it was shown that streamwise gradients of surface temperature reliably mark the mean separation point (at the

maximum gradient) and the transition point (at the minimum gradient). The location of the mean reattachment was found to align precisely with the minimum surface temperature location.

The present work is aimed at improving knowledge about the use of IRT for LSB detection on airfoils in steady and dynamic flow conditions, extending the investigation by Wynnychuk and Yarusevych.[18] The choice of the NACA 0018 airfoil is motivated by its symmetric geometry, which avoids camber effects, and its relatively large thickness, which promotes the formation of well-defined laminar separation bubbles at low Reynolds numbers. Moreover, its extensive use in previous studies enables direct comparison with existing datasets. As a first step in this work, the authors focused their attention on investigating the accuracy of algorithms available in the literature applied to surface temperature measurements for the quantitative assessment of LSB characteristics (separation, transition, and reattachment) in steady-state conditions. This involved comparing the locations of the IRT-detected fronts, as analyzed from dewarped visualization images, with the primary reference front locations identified through classical China Clay surface flow visualization. Therefore, the main goal of the present activity was to comprehensively extend the characterization of LSB features for the NACA 0018 airfoil into unsteady, periodic flow regimes, specifically investigating pitching motions at various reduced frequencies with different amplitudes of the oscillation cycle, through the application of the DIT technique. In particular, this study was designed to evaluate the capability of infrared thermography measurements to accurately capture the hysteresis of LSB characteristic point positions as a function of the sinusoidal pitching cycle parameters and flow regime, moving beyond the transition-point-only limitation found in earlier literature.

II. EXPERIMENTAL SET UP

A dedicated pitching airfoil test rig was designed and installed at the Green Wind Tunnel of the Aerodynamics Laboratory in the Department of Aerospace Science and Technology (DAER) of Politecnico di Milano (POLIMI). The wind tunnel test section measures 1 (length) × 0.3 (width) × 0.45 m^3 (height), and the maximum flow velocity achievable is 36.5 $m\,s^{-1}$ with turbulence level below 0.35%. The complete setup of the IRT experiments on the pitching airfoil test rig is shown in Fig. 2.

The airfoil model consists of a straight rectangular wing featuring a NACA 0018 airfoil, with chord $c = 100$ m and span $b = 300$ mm. It is manufactured via 3D printing using Acrylonitrile Styrene Acrylate (ASA) filament [thermal conductivity, $\lambda = 0.16$–0.21 ($W\,m^{-1}\,K^{-1}$), specific heat capacity, $C_p = 1300$ ($J\,kg^{-1}\,K^{-1}$)]. By comparing the material's thermal properties surveyed in the work by Gardner *et al.*,[9] ASA was selected as being suitable for IRT measurements, particularly for providing appreciable signal peaks in the surface temperature gradient maps, allowing an accurate evaluation of the boundary layer transition position. Moreover, in order to minimize reflections during the experiments, the model has been coated with a black matte paint. The airfoil model was printed with 100% infill to enhance structural robustness and avoid deformation under aerodynamic loading. A through-hole, centered at the airfoil quarter chord, was included in the model design to accommodate a glued threaded bar, allowing the wing to be supported and connected to the pitching rig servomotor. The airfoil surface includes eight equally

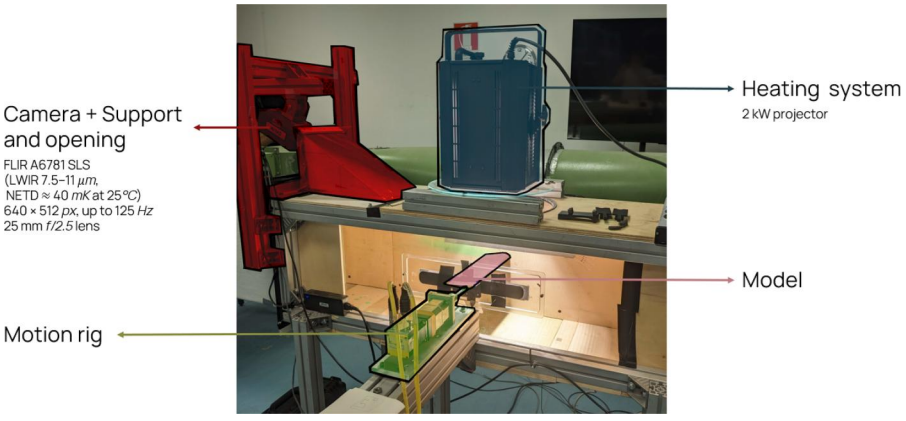

FIG. 2. Infrared thermography experimental set-up on pitching airfoil test rig at DAER POLIMI Green Wind Tunnel.

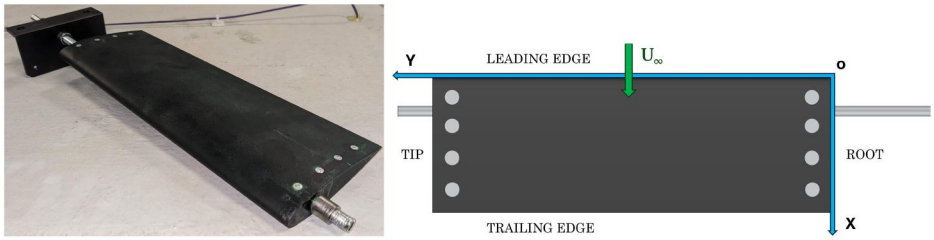

(a) View of the NACA 0018 model (b) Model Reference System

FIG. 3. NACA 0018 airfoil model with fiducial markers and support.

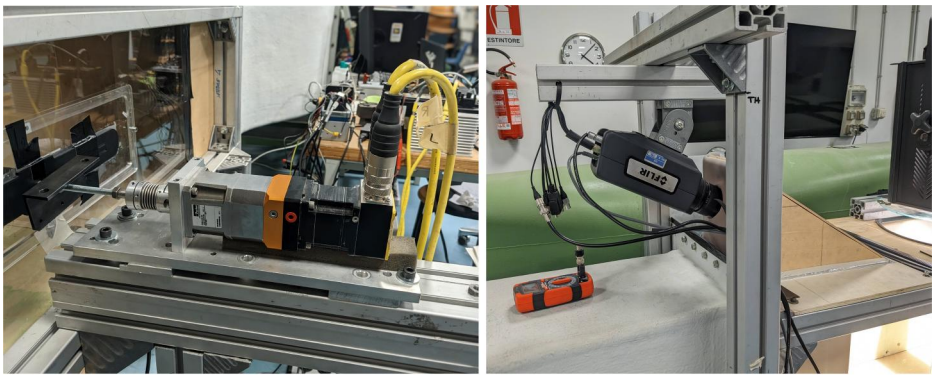

(a) Servomotor coupled with gear-box (b) LWIR Infrared Camera

FIG. 4. Particulars of the motion rig and imaging system.

spaced fiducial markers of diameter $d = 5$ mm made of aluminum tape [see Fig. 3(a)]. The markers are divided into two rows of four, with a chordwise distance between two consecutive markers of 20 mm. They are attached near the model edges to avoid forced transitions within the imaging region. The model reference system $X - Y$ used to present IRT results is shown in Fig. 3(b).

A dedicated motion system was specifically designed and employed for these tests to perform sinusoidal pitching cycles of the airfoil around its quarter chord [see Fig. 4(a)]. The motion system was composed of a Parker BE231DQ-NPSN servomotor coupled with a Parker FX60-040-S2 40:1 gearbox, a Parker Aries AR-04AE servo drive, and a Parker ACR 9000 motion controller module. A pitching motion control routine, based on the angular feedback of the airfoil provided by the encoder built into the servomotor, was implemented in *LabVIEW*. The encoder resolution, reaching 8000 pulses per revolution, granted an input precision of 0.045°. The motion rig can prescribe a sinusoidal cycle of the airfoil model angle of attack (α) according to

$$\alpha = \bar{\alpha} - \hat{\alpha}\sin(2\pi f t), \tag{1}$$

where the mean angle $\bar{\alpha}$, the oscillation amplitude $\hat{\alpha}$, and the pitching frequency f can be adjusted by the user.

A 2 kW Fresnel projector was used to guarantee a constant heat flux through the tempered glass on the ceiling of the test section. The projector was placed with its internal lamp at a height of 490 mm above the airfoil model. As shown in Tomasello,[20] this lamp positioning was considered the best option for the present setup, allowing for a chordwise constant temperature increase in the model surface of 8–10 K, which is suitable for accurate IRT measurements of BL transition.

Image acquisition was performed using a FLIR A6781 SLS longwave infrared camera (LWIR) that features a cooled strained-layer superlattice detector operating in the 7.5–11 μm spectral range. The thermal sensitivity is limited by a noise-equivalent temperature difference of 40 mK at 25 °C. The device has a maximum resolution of 640 × 512 px with a frame rate of up to 125 Hz at full resolution. The camera was equipped with a 25 mm, f/2.5 lens and was installed externally at the end of the test section, held by a support system composed of a modular structure consisting of four aluminum frames and an adjustable mount [see Fig. 4(b)]. This design allows for the adjustment of the height, horizontal position, and viewing angle to achieve the desired field of view (FOV) that covers the area over the airfoil upper surface of the model. The camera was focused on the center of the FOV when the airfoil was at zero incidence. The thermal loads experienced by the model during the experiments were limited, and no visible degradation or variation in the thermographic response was observed over the duration of the campaign. Although no direct roughness measurements were performed, these conditions suggest that the surface properties remained stable and did not significantly affect the LSB development.

Surface flow visualizations were conducted in steady-state flow conditions by painting the model surface with China Clay powder. When the paint pattern reached a steady condition, photographs of the model's upper surface were taken using a regular camera with 12 MPx resolution. The camera was positioned upstream with respect to the model to visualize the streaklines, including those in the region near the airfoil leading edge. The paint-drying fronts revealed the separation, transition, and reattachment positions of the LSB over the airfoil surface, enabling a primary direct comparison with the IRT imaging (see Fig. 5). Indeed, in China Clay flow visualizations, the reattachment location is associated with the downstream drying front, which marks the onset of increased wall shear stress and convective transport as the turbulent shear layer reattaches to the surface.

A. Test matrix

The experimental campaign included measurements in static conditions using the classical IRT technique and surface flow

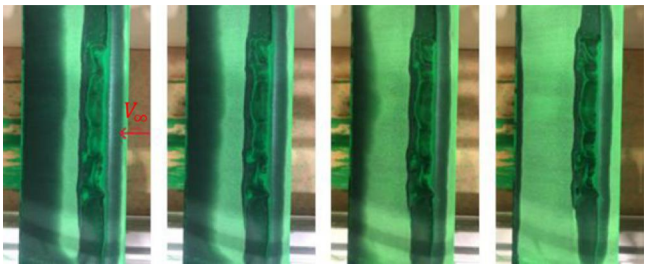

FIG. 5. Paint drying fronts develop over the upper surface of the model during China Clay flow visualizations for $\alpha = 6°$.

TABLE I. Test matrix of the experimental campaign.

	Steady	Unsteady
Infrared technique	IRT	DIT
Mean angle of attack $\bar{\alpha}$ (deg)	[0, 2, 4, 6, 8, 10]	5
Pitch amplitude $\hat{\alpha}$ (deg)	···	±[2, 3, 4, 5]
Reynolds number Re	80 000, 120 000	80 000, 120 000
Pitch frequency f (Hz)	···	[1, 2, 3, 4, 6]
Reduced frequency $k = \pi fc/U_\infty$	···	[0.0172, 0.1047]
Number of infrared images	800	3300
Acquisition frequency (Hz)	40	100

visualizations, aimed at validating the setup against results available in the literature for the same airfoil and flow conditions[18] and performing a quantitative assessment of IRT techniques to evaluate the positions along the airfoil chord of the LSB characteristic points (separation, transition, and reattachment). Steady measurements involved the acquisition of 800 thermal images at 40 Hz for each angle of attack tested in the range between $\alpha = 0°$ and 10°.

Unsteady pitching conditions consisted of sinusoidal cycles with a mean angle of attack $\bar{\alpha}$ equal to 5° and an oscillation amplitude $\hat{\alpha}$ between 2° and 5°. Unsteady measurements involved the acquisition of 3300 thermal images at 100 Hz for each investigated cycle. Steady and unsteady measurements were performed at two Reynolds numbers, i.e., 80 000 and 120 000. The complete test matrix of the experimental campaign, reporting the test parameters, is shown in Table I.

III. IRT IMAGE ANALYSIS

The thermal images were analyzed by an in-house MATLAB code implementing DIT technique. Details about the image processing code can be found in Tomasello and Poletti, M.Sc. Dissertations.[20,21]

The thermal images were mapped onto a three-dimensional grid by automatically detecting the fiducial markers [see Fig. 6(a)] and then dewarped onto a 2D surface to view the model's upper surface [see Fig. 6(b)]. Considering the geometrical coordinates of the NACA 0018 airfoil, the model geometry for the thermal images is discretized on a structured grid using 0.25 mm/node spacing along both chordwise and spanwise directions. This choice ensures that the mapping of thermal images onto the grid preserves all intensity details without loss of resolution. As shown in Fig. 6, the same mapping and dewarping procedure was applied to the China Clay visualization images to allow a direct comparison of the two techniques for the detection of the LSB characteristic points. Figure 6 shows how the LSB characteristic points can be recovered from the paint-drying fronts observed in the China Clay surface visualizations. In particular, a transition occurs where a change in the China Clay pattern is observed before reattachment.

A mean spatial filter with 0.5 × 0.5 mm size, which corresponds to a 3 × 3 node window, was applied to the dewarped thermal images to reduce pixel-level noise.[22] For steady-state airfoil IRT measurements, all the 800 images acquired at each angle of attack were averaged into a single thermal intensity map, allowing for a higher signal-to-noise ratio (SNR) with respect to an individual image.[23,24] For the unsteady IRT measurements, the simultaneous acquisition of the airfoil angle of attack time history enabled the grouping of the thermal images collected along the pitching cycle into a number of bins with an incidence amplitude of 0.5°, separately for the upstroke and downstroke phases of the motion. Then, the grouped thermal images were bin-averaged to obtain a single image associated with the mean angle of attack of the bin. The choice of an incidence bin width of $\Delta\alpha = 0.5°$ represents a compromise between angular resolution and signal-to-noise ratio. Indeed, a smaller bin led to noisier intensity distributions that could provide less robust identification of the characteristic points. To apply DIT, the differential thermal intensity ΔI is computed using a sliding window approach, whereby averaged thermal images corresponding to consecutive angles of attack, $\Delta\alpha = \alpha_2 - \alpha_1$, are subtracted along the pitching cycle. In particular, $\Delta\alpha$ values equal to 0.5° and 1° were tested for DIT evaluations of the LSB characteristic points' locations in static airfoil conditions, while $\Delta\alpha = 1°$ was used for the pitching airfoil conditions, as this latter choice led to obtaining a consistent increase in the SNR in the present setup, while producing negligible measurement phase lag relative to the instantaneous angle of attack.[9]

Then, a region of interest (ROI) was selected from the dewarped thermal images to exclude areas where three-dimensional aerodynamic features or local variations of the thermal map could compromise the reliability of the results in terms of LSB characteristic points detection. As a matter of fact, the averaged thermal images revealed that the central portion of the model is characterized by nearly two-dimensional flow behavior, while three-dimensional effects become significant in the vicinity of the edges (see Fig. 6). For this reason, under all test conditions, the spanwise Y boundaries of the ROI were fixed between 70 and 230 mm.

The chordwise intensity distributions were averaged along the spanwise extent of the ROI and smoothed to reduce the noise level using a cubic spline interpolation,[25] resulting in a single chordwise intensity profile. Sample smoothed chordwise intensity profiles obtained by applying classical IRT and the DIT technique to the present steady airfoil measurements are shown in Fig. 7. While this averaging approach enhances robustness and reduces noise, it inherently filters out spanwise variations of the flow. As a consequence, possible three-dimensional or non-uniform structures in the leading-edge region under unsteady conditions are not explicitly captured, although they remain qualitatively observable in the raw thermographic fields.

For static airfoil conditions, the characteristic LSB points' positions were retrieved from the smoothed intensity distribution I, as done in Wynnychuk and Yarusevych.[18] In particular, as depicted in Fig. 7(left), the separation point was retrieved at the maximum slope of the chordwise intensity distribution, the transition point at the minimum slope, while the reattachment point was retrieved as the minimum of the chordwise intensity distribution downstream of transition. Moreover, alternatives for reattachment point detection were considered for static airfoil measurements, i.e., the *intersection point method*,[10,25], which considers the intersection point between the tangent line through the transition point and the one through the first inflection point encountered downstream of transition; and the *maximum curvature point method*, which considers the point of maximum intensity curvature downstream of transition.[25]

On the other hand, for DIT analysis, the LSB characteristic points' locations can be evaluated from the intensity difference

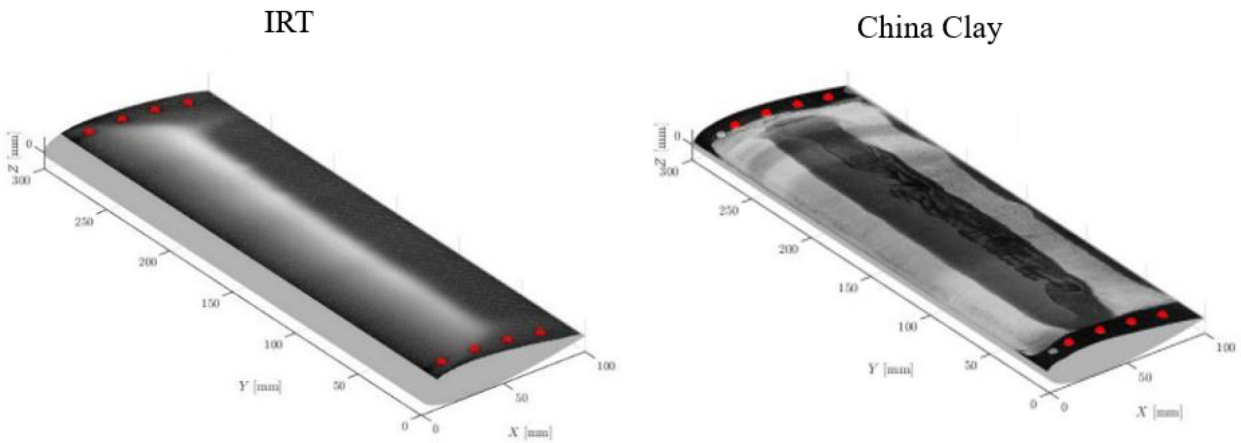

(a) Airfoil 3D mapped images

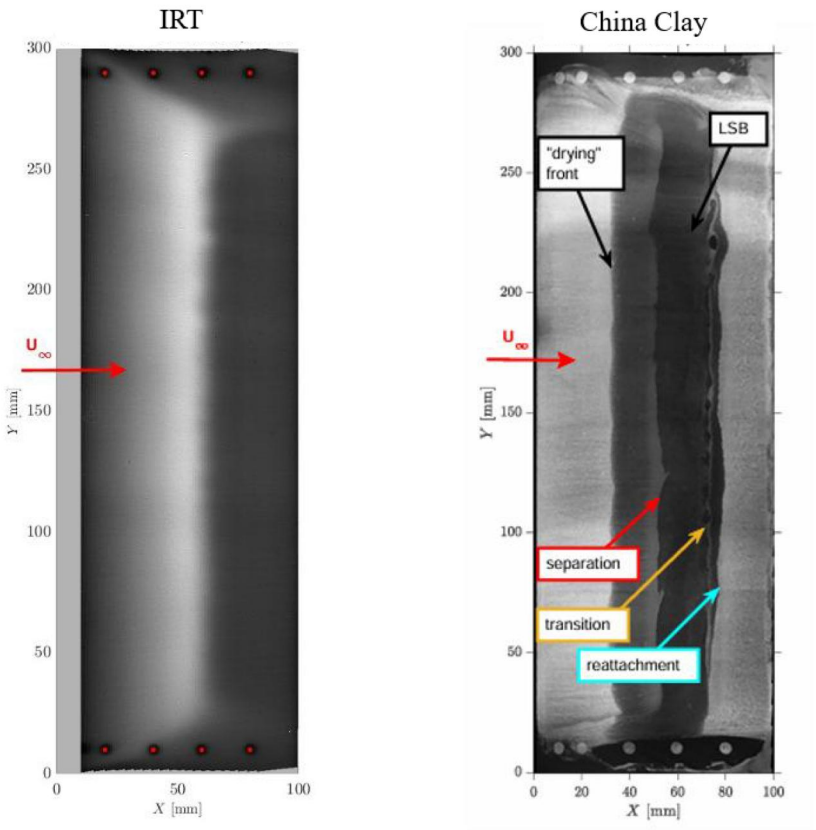

(b) Airfoil upper surface 2D dewarped views

FIG. 6. Comparison of sample three-dimensional and 2D dewarped reconstructed images of the NACA 0018 airfoil obtained using IRT and China clay visualizations.

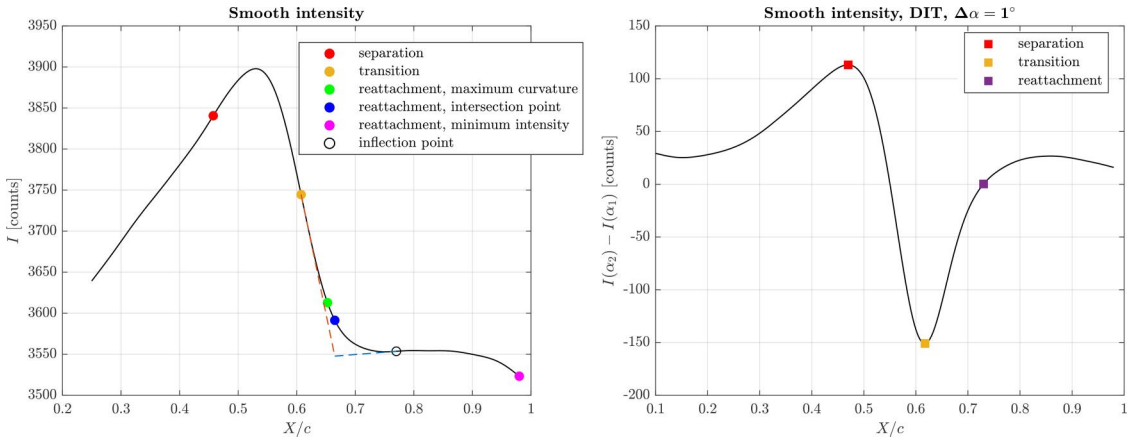

FIG. 7. Identification of LSB characteristic points from the intensity distributions of average thermal images obtained for IRT and DIT in static airfoil conditions.

distribution ΔI, as reported in Grille Guerra *et al.*[19] In particular, the separation point can be identified at the maximum peak of the ΔI profile, the transition point at the minimum peak of ΔI, while the reattachment point is found where ΔI changes sign downstream of transition [see Fig. 7(right)].

Nevertheless, the DIT chordwise intensity distributions obtained for the present measurements in unsteady oscillating conditions show the maximum peak at the airfoil leading edge coordinate across all the angles of attack considered in the investigated pitching cycles, as shown by the sample profile depicted in Fig. 8. This outcome is in accordance with the results obtained by Wolf,[10] suggesting that the method for identifying the LSB separation point from DIT in steady-state flow conditions could be inadequate for pitching airfoil measurements. As a matter of fact, the current camera configuration, positioned downstream of the airfoil with a highly inclined viewing angle, reduces the effective spatial resolution near the leading edge, particularly during the upstroke at higher angles of attack. This also may be a factor that contributes to the difficulty in identifying the separation location. In this context, the use of an additional camera with a more orthogonal perspective to the leading-edge region could significantly improve the detection of separation features. Therefore, the present DIT technique was used to evaluate the effects of pitching motion amplitude and reduced frequency on the positions of the LSB transition and reattachment points. In particular, the investigation of the LSB reattachment point behavior under pitching airfoil conditions represents a novelty of the present work beyond the state of the art.[10,19]

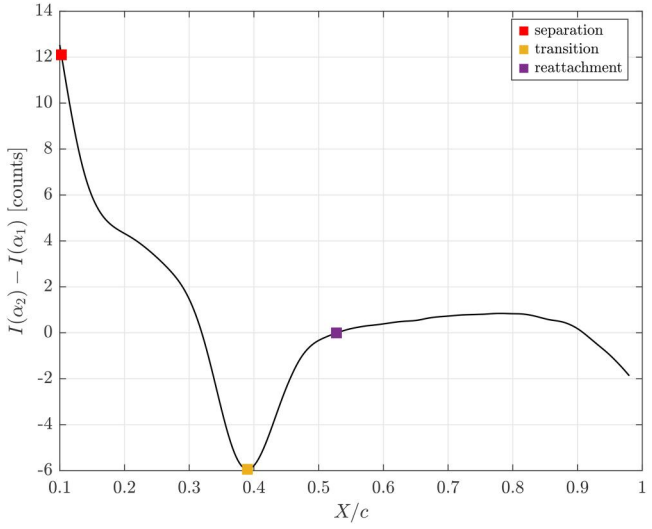

FIG. 8. Identification of LSB characteristic points from the intensity distribution of average thermal images obtained from DIT in pitching airfoil conditions.

IV. RESULTS AND DISCUSSION

A. Static airfoil conditions

The results analysis starts with the discussion of the measurements performed with the airfoil in static conditions which, as mentioned earlier, were primarily focused on a quantitative assessment of IRT techniques and best practices used to investigate the LSB characteristic points' positions. With this aim, Fig. 9 shows a comparison of the separation, transition, and reattachment positions evaluated by the present IRT measurements, including the DIT technique, for different airfoil angles of attack at $Re = 120\,000$. Similar outcomes can be deduced from the comparison of results at $Re = 80\,000$, which therefore are not presented for the sake of brevity. The points' positions were superimposed onto the dewarped top view obtained from the China Clay surface flow visualizations to provide a primary validation of the methods employed for point detection from thermal images. Moreover, results obtained from the reference work by Wynnychuk and Yarusevych[18] over the same airfoil were also included for comparison.

For all the angles of attack tested, the separation point in the current experiment occurs slightly further downstream than in the reference work,[18] but the positions evaluated with the present IRT and DIT measurements show quite good agreement with flow visualization. This confirms the suitability of the infrared thermography technique for accurately capturing the flow physics features related to the generation of the LSB in the present setup. Indeed, the discrepancies

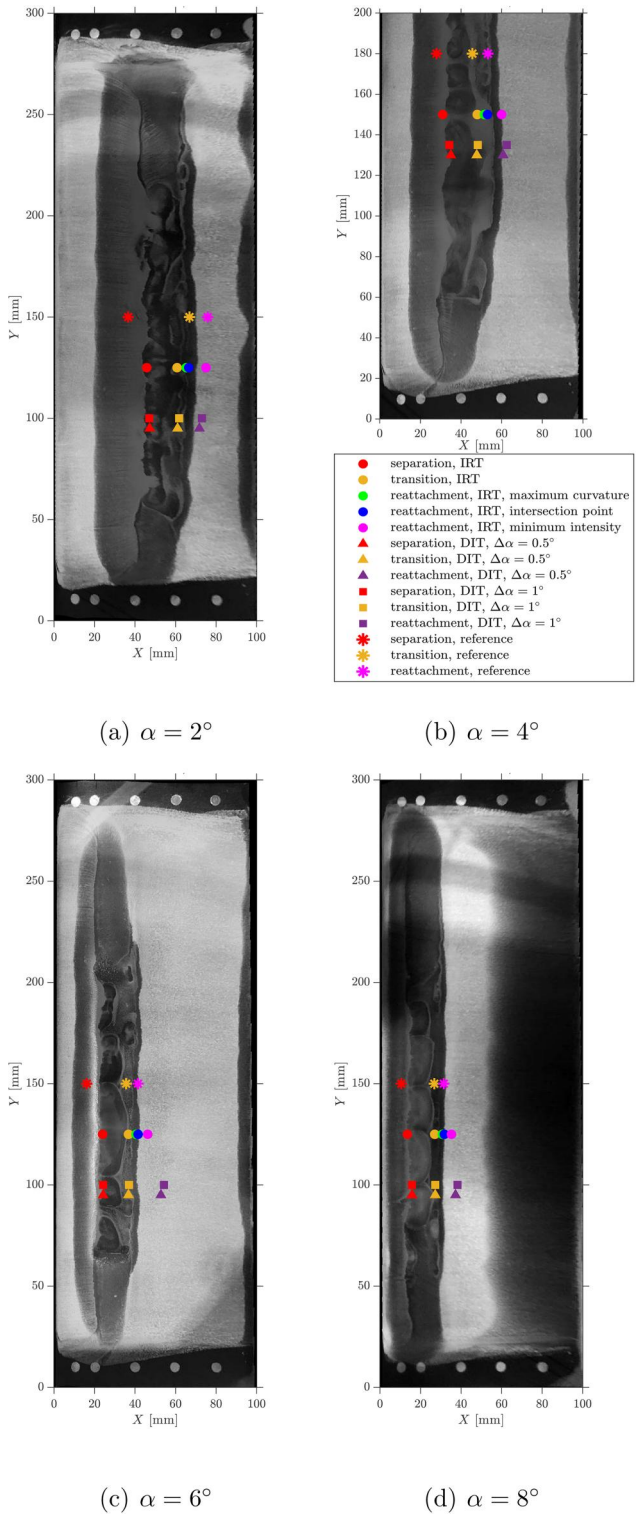

FIG. 9. Comparison between the LSB characteristic points location evaluated for static airfoil conditions with infrared thermography techniques and China Clay flow visualizations, $Re = 120\,000$, reference IRT by Wynnychuk and Yarusevych.[18]

observed with respect to the characteristic points' locations evaluated in the reference work could be related to differences in the airfoil setup and in the wind tunnel flow characteristics employed,[18] which could slightly alter the physics related to the generation and the extent of the LSB occurrence on the airfoil. Generally, the separation point locations computed applying DIT, both with $\Delta\alpha = 0.5°$ and 1°, show a satisfactory agreement with flow visualizations at all angles of attack. In particular, a slight discrepancy between IRT and DIT results can be observed at $\alpha = 4°$, where the IRT result is slightly closer to the visualization outcome, while DIT predicts a separation position slightly further downstream.

The transition point locations evaluated by the present IRT measurements are also in quite good agreement with flow visualizations across all the investigated angles of attack. Analogously to what was found for the separation point, transition locations calculated applying DIT using both $\Delta\alpha$ variations show a satisfactory agreement with flow visualizations, even as the angle of attack increases.

Concerning the reattachment point location computed applying IRT, generally, the intersection point method between tangent lines shows the best agreement with flow visualizations at all angles of attack. Indeed, the minimum point method shows a reattachment occurring slightly downstream of the flow visualizations. Moreover, the maximum curvature point method provides results quite close to the intersection point method, with the two points being hardly distinguishable in the images for all the angles of attack. The reattachment point evaluation computed applying DIT shows the highest discrepancies from visualizations, in particular at $\alpha = 6°$ and 8°, thus suggesting the lower robustness of the differential technique for identifying this specific characteristic point in steady flow conditions compared to classical IRT methods. While the intersection point method provides accurate reattachment estimates in steady conditions, its application to unsteady DIT data are not straightforward. The differential intensity distributions obtained under pitching conditions are often characterized by lower gradients and increased noise levels, which hinder the robust identification of inflection points and tangent directions required by geometric methods. For this reason, feature-based criteria are directly applied to the ΔI signal, such as the zero-crossing approach, will be adopted for unsteady cases.

Finally, Table II reports the quantitative positioning of the LSB characteristic points evaluated by IRT in steady conditions at $Re = 120\,000$.

TABLE II. Position of the LSB characteristic points evaluated by IRT in steady conditions at $Re = 120\,000$. The reattachment point is computed with the intersection point method.

α (deg)	Separation X/c	Transition X/c	Reattachment X/c
0	0.48	0.73	0.80
2	0.46	0.61	0.67
4	0.31	0.48	0.53
6	0.24	0.37	0.42
8	0.14	0.27	0.32
10	0.10	0.21	0.25

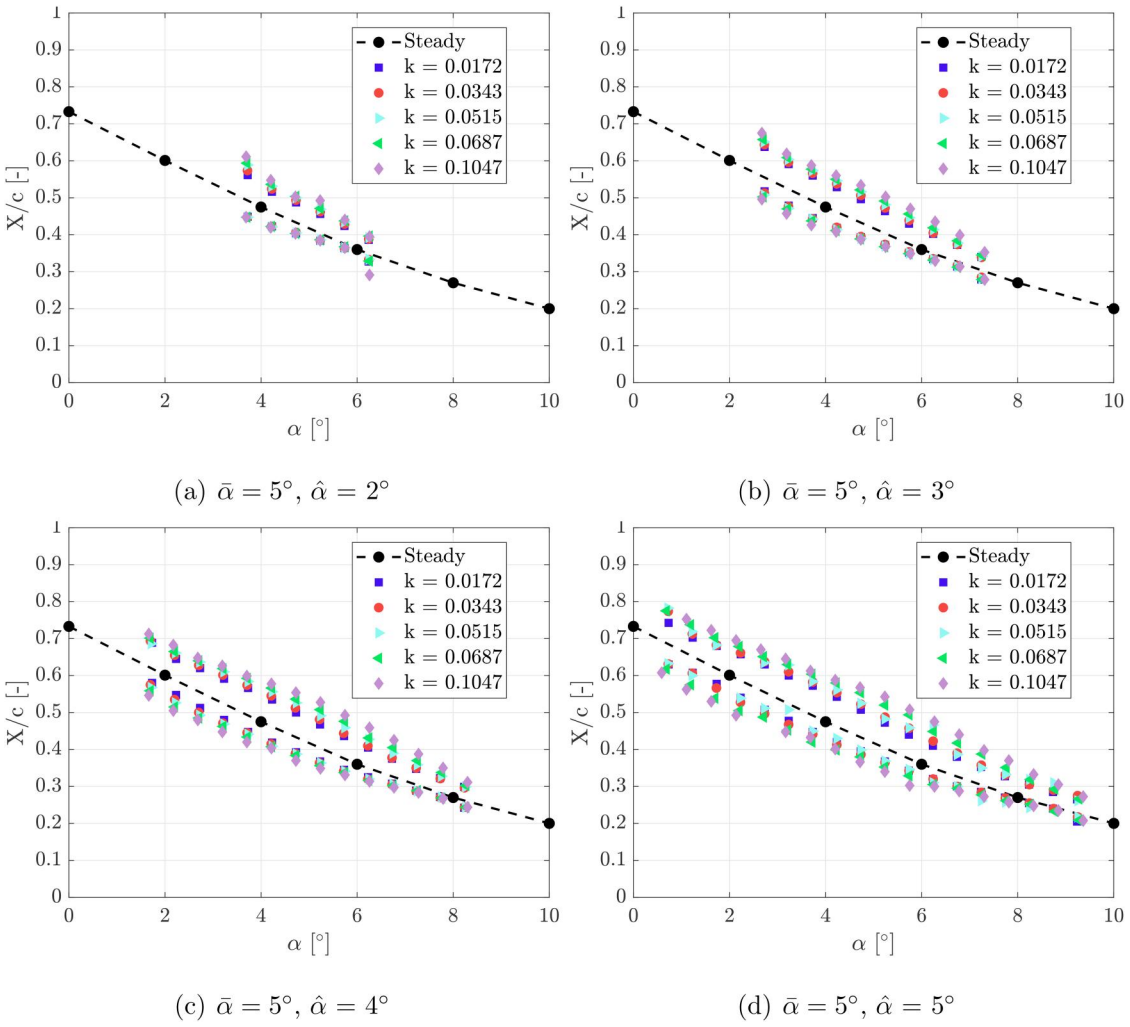

FIG. 10. Comparison of the LSB transition point locations evaluated by DIT by varying reduced frequency k, $\bar{\alpha} = 5°$, $Re = 120\,000$.

B. Pitching airfoil conditions

The positions of the LSB characteristic points evaluated using DIT are now discussed for pitching airfoil conditions to evaluate the effects of different pitching frequencies and cycle amplitudes. As reported in the test matrix (see Table I), while the mean angle of the sinusoidal cycle was fixed at $\bar{\alpha} = 5°$, the pitching amplitude varied from $\hat{\alpha} = 2°$ to $5°$ in order to progressively cover the angle of attack range investigated in the static measurements. Moreover, the range of tested pitching frequencies allowed for the investigation of both quasi-steady (i.e., reduced frequency $k < 0.05$) and unsteady regimes (i.e., $0.05 < k < 0.1$), with the latter reproducing the characteristic reduced frequencies investigated for blade dynamic stall.[26,27] In the present work, no continuous sweeps between increasing and decreasing values were performed. Therefore, hysteresis with respect to reduced velocity cannot be directly assessed. However, its influence is reflected in the modification of the hysteresis loops observed over the pitching cycle, with increasing reduced velocity affecting both the amplitude and shape of the characteristic point trajectories. Indeed, from a physical standpoint, the pitching cycle can be interpreted as a continuous variation of the effective reduced velocity, thus allowing the observed upstroke and downstroke paths to be interpreted as increasing and decreasing reduced velocity conditions, respectively.

In the following, the LSB point locations obtained for static angles of attack are plotted on the same graphs used to present results for pitching conditions to provide a clear evaluation of the dynamic effects. In particular, the reattachment point under static conditions is evaluated using the intersection point method, as it showed the best agreement with flow visualizations as described before. The results discussion will be focused on tests performed at $Re = 120\,000$, while results obtained at a lower Reynolds number, i.e., $Re = 80\,000$, will be discussed for a single oscillation cycle characterized by a mean angle of attack $\bar{\alpha} = 5°$ and amplitude $\hat{\alpha} = 4°$, varying the reduced frequency in the same range tested at the higher Reynolds number. As discussed in Sec. III, the separation point location will not be

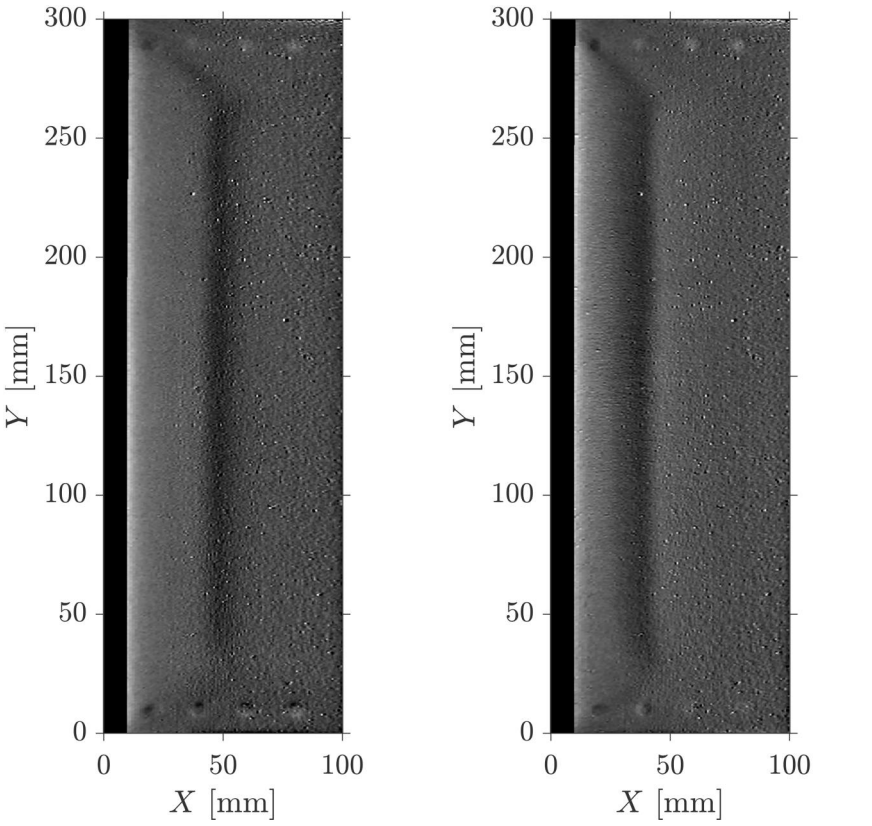

FIG. 11. Comparison of DIT images at the same angle of attack $\alpha = 4.75°$ in the upstroke and downstroke motion, $\bar{\alpha} = 5°$, $\hat{\alpha} = 4°$, $k = 0.0515$, and $Re = 120\,000$.

considered in the results analysis for pitching conditions due to the absence of a clear peak occurring before transition in the DIT chordwise intensity distributions (see Fig. 8).

1. Effect of pitching frequency

The transition point locations evaluated by DIT for the pitching cases with $\bar{\alpha} = 5°$ and $\hat{\alpha}$ in the range between 2° and 5° are compared in Fig. 10 to show the dependency of their locations with respect to the reduced frequency of the oscillating cycle.

As clearly shown, the transition point locations evaluated in unsteady conditions do not resemble the positions obtained under steady conditions; rather, a hysteresis loop is obtained around the curve traced by the steady results. In particular, the hysteresis denotes that the LSB transition points are located at the same chordwise X/c station at larger instantaneous angles of attack during the upstroke than during the downstroke. Indeed, the evolution of the laminar separation bubble over the pitching cycle exhibits a clear dependence on the direction of motion. During the upstroke, the increasing adverse pressure gradient promotes earlier separation and delayed transition, resulting in an elongated LSB and a downstream shift of the reattachment point. During the downstroke, the boundary layer recovers progressively, leading to a shorter LSB. However, this recovery is not instantaneous, giving rise to a delayed upstream movement of the characteristic points. This asymmetry results in a pronounced hysteresis, reflecting the non-equilibrium nature of the boundary layer response.

As a measure of the hysteresis magnitude, the difference in the characteristic point locations evaluated in upstroke and downstroke with respect to static measurements can be considered. Using this metric, a more evident hysteresis was found during the upstroke, becoming stronger as the reduced frequency k increases. Indeed, during the downstroke, the transition points' locations follow almost the same path obtained in static conditions, showing a slight hysteresis with respect to reduced frequency. This behavior is common to all investigated pitching conditions characterized by increasing oscillation amplitude $\hat{\alpha}$.

In order to highlight the presence of the hysteresis behavior of the transition point in unsteady conditions, Fig. 11 compares sample DIT images evaluated at the same angle of attack $\alpha = 4.75°$ in upstroke and downstroke motion for the pitching cycle $\bar{\alpha} = 5°$ at a single reduced frequency.

In particular, the dark region of the DIT images, highlighting qualitatively the area around the local minimum associated with the transition, shifts its position between the upstroke and downstroke phases at the same angle of attack of the pitching cycle. Indeed, considering the thermal footprints of the markers as a qualitative spatial reference for the transition area, Fig. 11(a) shows that the dark region

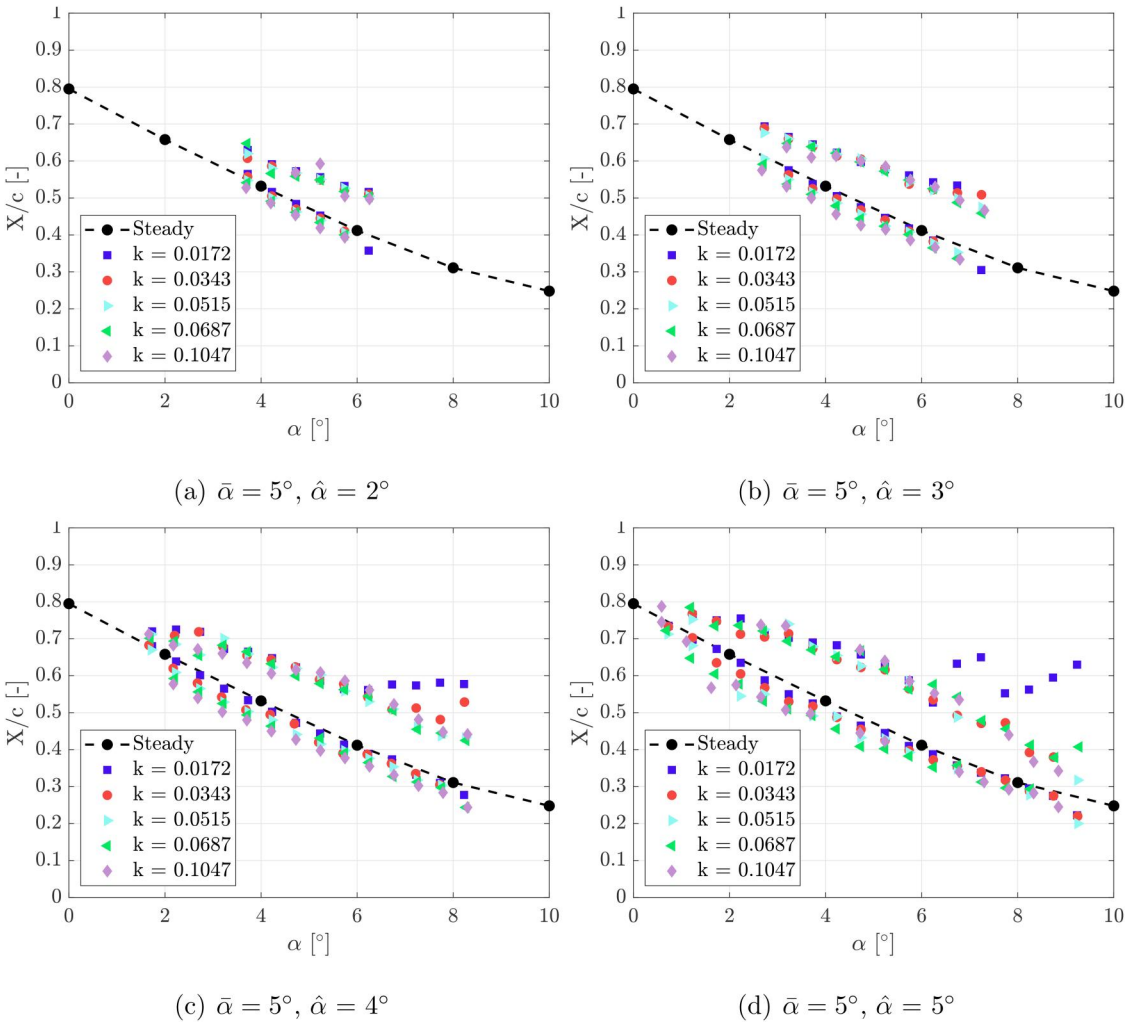

FIG. 12. Comparison of the LSB reattachment point locations evaluated by DIT by varying reduced frequency k, $\bar{\alpha} = 5°$, $Re = 120\,000$.

apparently lies between the second and the third marker in the upstroke, whereas in the downstroke, it aligns roughly with the second marker [see Fig. 11(b)]. This representation confirms the flow physics related to the hysteresis of the transition point with respect to the phase of the pitching motion under unsteady conditions. In particular, this hysteresis is augmented as the pitching frequency increases. Indeed, according to Theodorsen's theory,[28] harmonically pitching airfoils exhibit hysteresis in the lift response with respect to the angle of attack. The aerodynamic force phase lag arises from the periodic shedding of vorticity generated in the wake, influencing the pressure distribution, where vortex strength varies sinusoidally with time. Concerning the transition position, the increase in hysteresis with respect to reduced frequency is a direct result of the unsteady pressure gradient failing to equilibrate with the viscous forces in the boundary layer. The higher the reduced frequency, the less time the boundary layer has to adapt, leading to a larger lag and thus a wider hysteresis loop in the transition location.[29,30]

The reattachment point locations evaluated by DIT for the same pitching cycles analyzed before are now compared in Fig. 12(a). The identification of the reattachment point in the present unsteady DIT analysis is based on the zero-crossing of the differential intensity distribution, consistently with common practice in the literature. Although alternative criteria, such as derivative- or curvature-based methods, could in principle be considered, they were found to be significantly more sensitive to noise in the present experimental conditions. This is particularly evident at low reduced frequencies, where the ΔI profiles exhibit very low gradients, leading to strong noise amplification when numerical differentiation is applied. The reattachment points show quite a similar hysteresis behavior, albeit more pronounced in the upstroke phase compared to the transition point analysis. During the downstroke, the reattachment points show a position quite similar to the one evaluated in steady conditions at the same angle of attack, thus confirming the lower hysteresis observed for the transition point in this phase of the motion. In particular, as

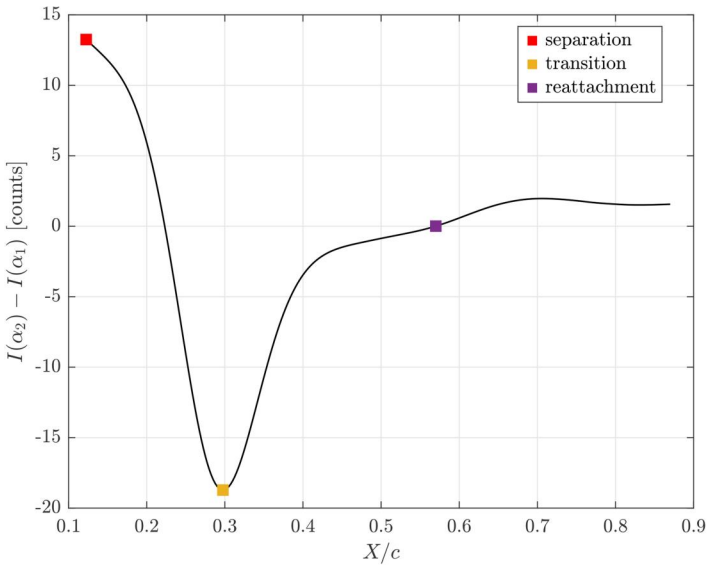

(a) $k = 0.0172$

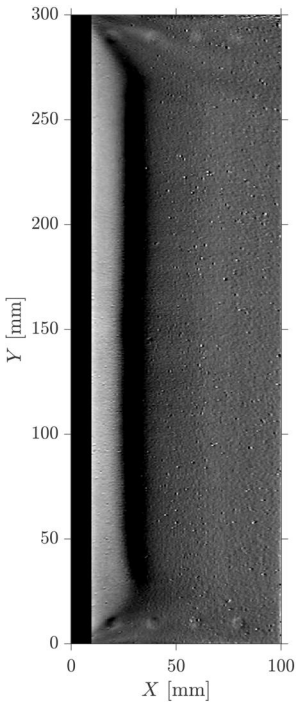

(b) $k = 0.0172$

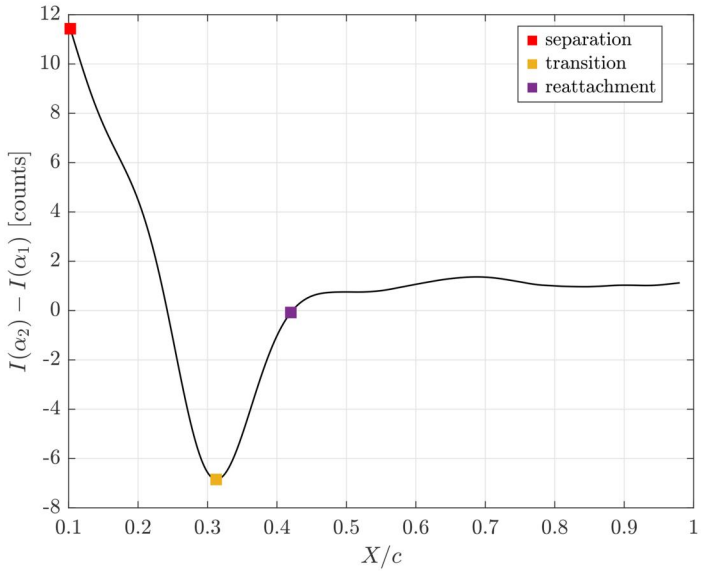

(c) $k = 0.1047$

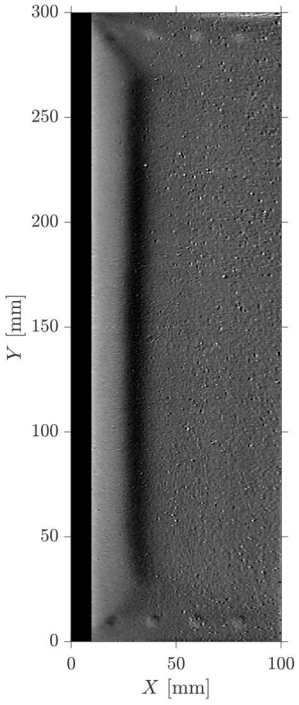

(d) $k = 0.1047$

FIG. 13. Comparison of the differential intensity distribution and DIT images at $\alpha = 6.75^\circ$ in upstroke, $\bar{\alpha} = 5^\circ$, $\hat{\alpha} = 4^\circ$, $Re = 120\,000$.

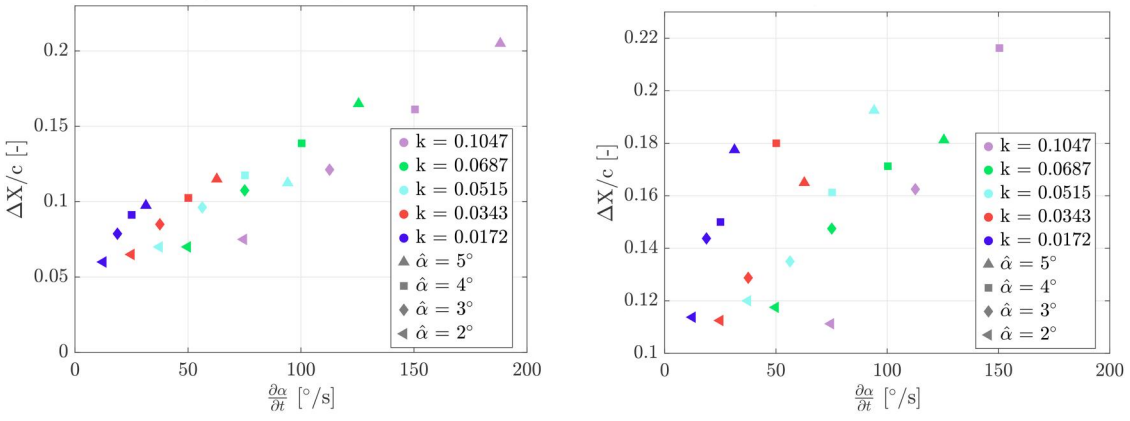

(a) Transition (b) Reattachment

FIG. 14. Comparison of the transition and reattachment point location hysteresis at $\alpha = 4.75°$ as a function of pitch rate, $Re = 120\,000$. Colors indicate data evaluated at different reduced frequencies k, while different markers indicate data acquired for different pitch cycle amplitudes $\hat{\alpha}$.

the angle of attack increases during the upstroke, the reattachment point shows increasing hysteresis with respect to the position evaluated in steady conditions at the same angles of attack. Moreover, for the pitching cycles with oscillation amplitudes $\hat{\alpha} = 4°$ and 5° and the lowest reduced frequencies, i.e., $k = 0.0172$ and 0.0343, the reattachment point position at high angles of attack in the upstroke shows a diverging trend toward the airfoil trailing edge.

A deeper understanding of this large divergence of the reattachment point position observed at low reduced frequencies in the upstroke can be achieved by analyzing the DIT images at a high angle of attack and the corresponding differential thermal intensity distributions. Figure 13 shows a comparison of the DIT images at $\alpha = 6.75°$ for the pitching cycle case with $\bar{\alpha} = 5°$ and $\hat{\alpha} = 4°$ at the lowest and highest reduced frequencies tested.

The reattachment point should be qualitatively recognized at the downstream edge of the darker region visible in the DIT images. However, at the lowest reduced frequency, it can be noticed that the differential intensity distribution changes sign further downstream than where the DIT image would suggest the reattachment point is positioned [see Figs. 13(a) and 13(b), respectively]. Indeed, the differential intensity distribution curve approaches the X/c axis with a quite low slope, thus intercepting the axis further toward the trailing edge with respect to what is shown in the thermal image. Moreover, the DIT image evaluated at the lowest reduced frequency shows two distinct shades of gray downstream of the darker area. In particular, the reattachment point location, identified where the differential intensity distribution changes sign, can be found at the end of the first gray shading. At the same angle of attack but at the highest reduced frequency ($k = 0.1047$), the differential intensity distribution curve intercepts the X/c axis with a higher slope, and thus further upstream [see Fig. 13(d)]. Consistently, in the corresponding thermal image, the intermediate gray shade is no longer observed; thus, the identification of the reattachment point is consistent with the flow physics revealed by the thermal image. This consistent behavior can also be observed in the thermal images evaluated at low angles of attack across the whole range of reduced frequencies tested (not included here for the sake of brevity), supporting the expected trend of the reattachment point position shown in Fig. 12(a).

The absence of complementary information, as pressure coefficient or skin friction distribution, from other techniques, such as particle image velocimetry (PIV) or surface flow visualization using pressure-sensitive paint (PSP), inevitably affects the capability to provide a robust flow physics interpretation of the apparent divergence of the reattachment points observed at high angles of attack during the upstroke at low reduced frequencies. Indeed, the observed divergent trend could be correlated with the onset of shear layer instabilities associated with the unsteadiness level of the flow, influencing the extension of the LSB along the airfoil, or to the possible occurrence of incipient stall phenomena due to the high adverse pressure gradient experienced by the boundary layer at high angles of attack toward the trailing edge region. This downstream divergence of the reattachment location observed at low reduced frequencies during the upstroke may be associated with enhanced shear layer instability growth under stronger adverse pressure gradients and a possible loss of coherence of the laminar separation bubble structure. Under these conditions, the reattachment process may become intermittent or weakened, making its identification based on DIT criteria less robust. Therefore, the apparent displacement toward the trailing edge may reflect both a physical elongation or partial breakdown of the LSB and limitations of the measurement methodology. Indeed, as shown by the analysis of the thermal images and differential thermal intensity distributions under these peculiar flow conditions, the identification of the reattachment point might also be influenced by factors not strictly related to flow physics. For instance, due to the employed optical setup, the acquired thermal images could be characterized by a higher level of noise. Moreover, the approach commonly used in the literature to identify the reattachment point, based on the change in sign of the DIT intensity distribution, could suffer from limited applicability under these flow conditions.

Generally, the present measurements indicate that the effect of increasing the pitching cycle reduced frequency at a fixed mean angle of attack is a clear strengthening of the hysteresis loop, particularly

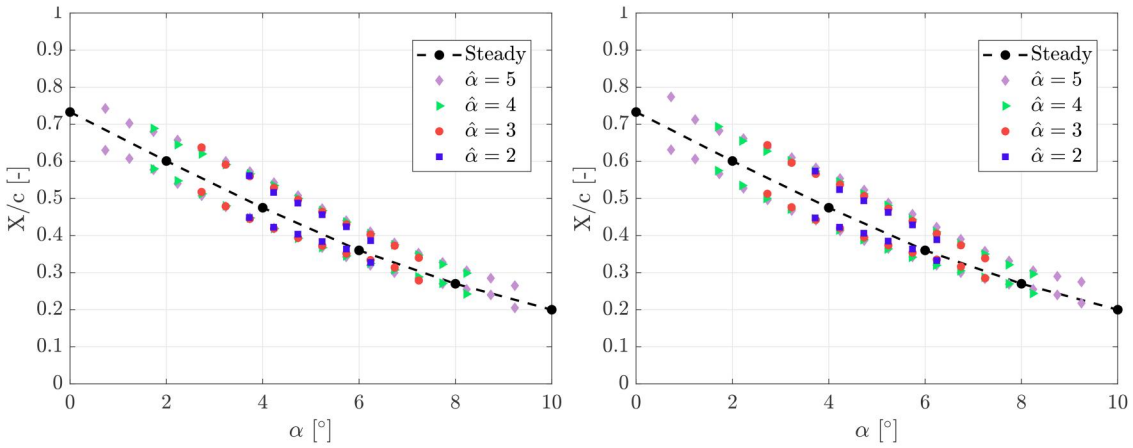

(a) $k = 0.0172$ (b) $k = 0.0343$

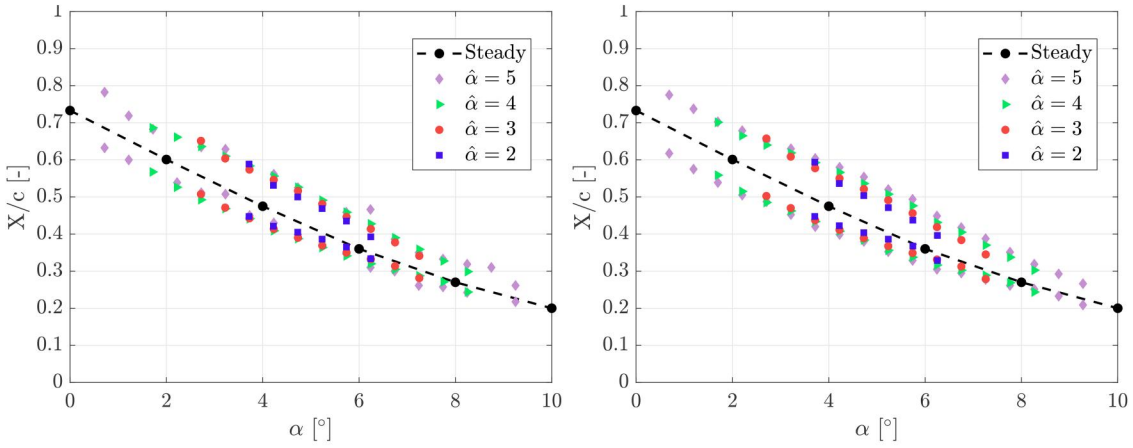

(c) $k = 0.0515$ (d) $k = 0.0687$

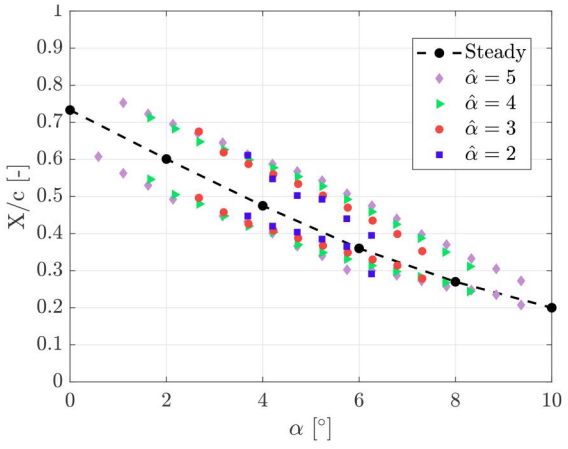

(e) $k = 0.1047$

FIG. 15. Comparison of the LSB transition point locations evaluated by DIT by varying pitching cycle amplitude $\hat{\alpha}$, $Re = 120\,000$.

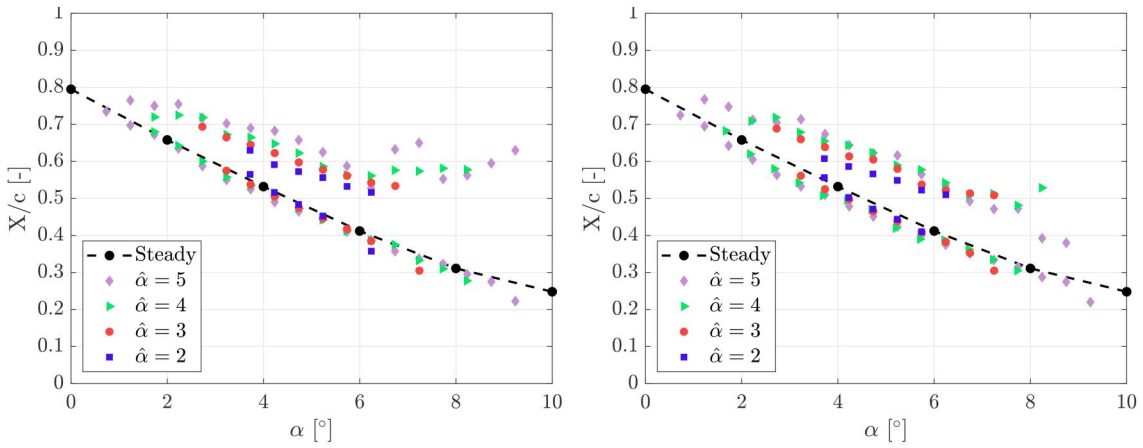

(a) $k = 0.0172$ (b) $k = 0.0343$

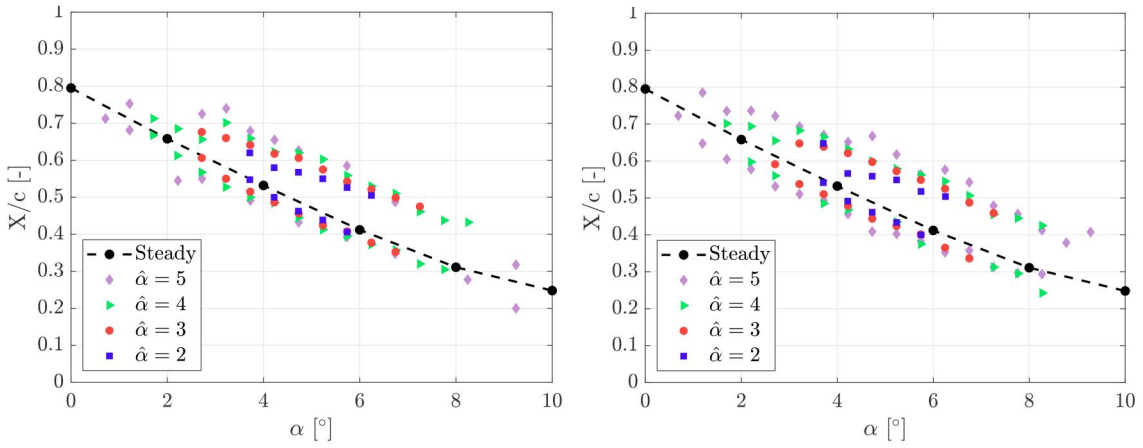

(c) $k = 0.0515$ (d) $k = 0.0687$

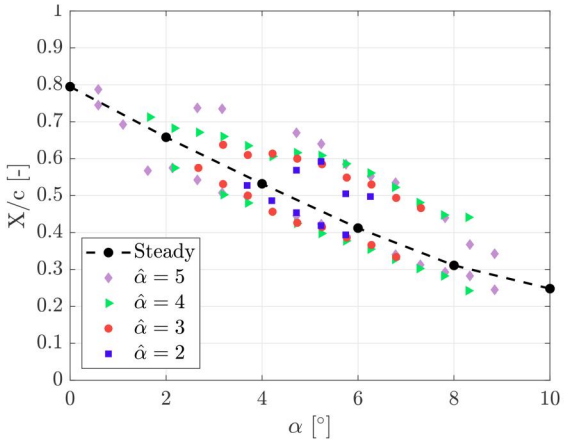

(e) $k = 0.1047$

FIG. 16. Comparison of the LSB reattachment point locations evaluated by DIT by varying pitching cycle amplitude $\hat{\alpha}$, $Re = 120\,000$.

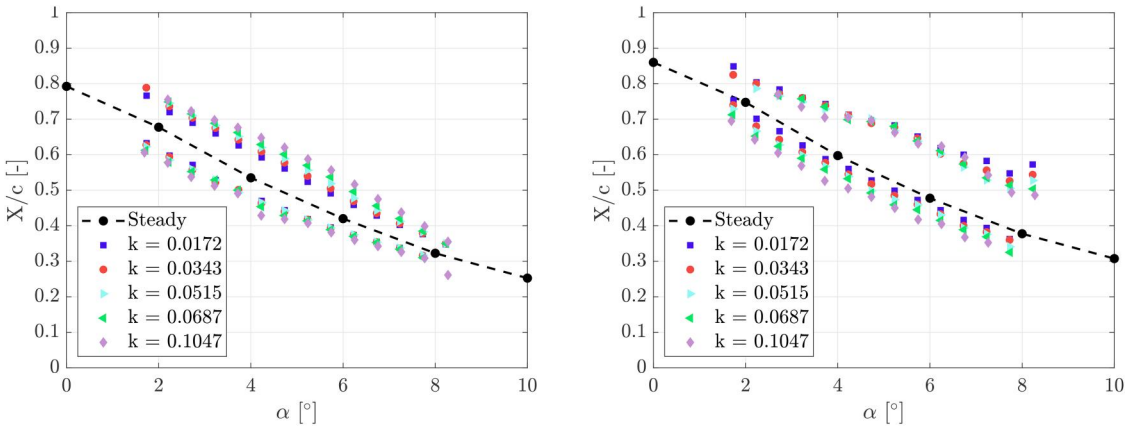

FIG. 17. Comparison of the LSB transition and reattachment point locations evaluated by DIT by varying reduced frequency k, $\bar{\alpha} = 5°$, $\hat{\alpha} = 4°$, and Re = 80 000.

during the upstroke phase. This behavior, well known for the transition point position and in agreement with the outcomes by Wolf *et al.*,[10] is here extended also to the reattachment point position. Indeed, the presence of the hysteresis observed for the reattachment point is compatible with the outcomes of Grille Guerra *et al.*,[19] based on pressure coefficient distribution measurements on a pitching airfoil at $Re = 200\,000$.

A quantitative comparison of the effect of reduced frequency on the LSB characteristic points' hysteresis can be obtained by plotting the difference of their chord-wise position between upstroke and downstroke $\Delta X/c = X_{upstroke}/c - X_{downstroke}/c$ with respect to the pitching rate[10] defined as

$$\frac{\partial \alpha}{\partial t} = 2\pi f \hat{\alpha} \cos(2\pi f t). \tag{2}$$

As a sample quantitative analysis, Fig. 14 shows the measured hysteresis $\Delta X/c$ of the transition and reattachment point location as a function of the pitch rate at a fixed angle $\alpha = 4.75°$ for all the investigated reduced frequencies and different pitch cycle amplitudes.

For transition point detection, the amount of hysteresis increases linearly as both the pitch rate and pitch cycle amplitude are increased [see Fig. 14(a)]. This trend is well in agreement with the results reported by Wolf *et al.*[10] and Weiss *et al.*[31] showing that transition point at a specific location scales linearly with $\frac{\partial \alpha}{\partial t}$. In addition, the present results confirm the same linear trend for the hysteresis of the reattachment point [see Fig. 14(a)].

2. Effect of pitching cycle amplitude

To highlight the influence of the pitch amplitude on the position of transition and reattachment points, DIT results obtained for the cycles with different pitching amplitude at the same reduced frequency are now compared, respectively, in Figs. 15 and 16.

Concerning the transition point, a negligible dependence of the hysteresis loop magnitude on the oscillation amplitude can be observed at low reduced frequencies. In contrast, a slight effect in terms of an increase in hysteresis can be observed when increasing the pitching cycle amplitude for higher reduced frequencies (i.e., $k = 0.0687$ and 0.1047), particularly during upstroke motion [see Figs. 16(d) and 16(e)].

Looking at the results obtained for the reattachment point, a similar behavior is observed, confirming a widening of the hysteresis loop as the pitching cycle amplitude increases. In particular, at the lowest reduced frequencies tested (i.e., $k = 0.0172$ and 0.0343), the divergent trend of the reattachment point position is apparent for the high angles of attack reached in the upstroke, with pitching cycle amplitudes $\hat{\alpha} = 4°$ and 5°. On the other hand, the divergence of the upstroke curves tends to vanish when observing DIT results obtained for the same pitching cycles at increased reduced frequencies, even if the curves' behavior seems slightly noisier with respect to the ones obtained for transition point detection.

3. Effect of Reynolds number

The IRT measurements performed at $Re = 80\,000$ for the pitching cycle with a mean angle of attack $\bar{\alpha} = 5°$ and amplitude $\hat{\alpha} = 4°$ enable the evaluation of the Reynolds number effect on the transition and reattachment point positioning at the different reduced frequencies tested. Before performing a direct comparison with the results obtained at $Re = 120\,000$, Fig. 17 collects the results obtained by DIT at $Re = 80\,000$ for the transition and reattachment points.

The results presented show that at the lower Reynolds number, both the transition and reattachment point curves are consistent with the features observed at $Re = 120\,000$. Indeed, as the reduced frequency increases, the transition point curves exhibit a widening of the hysteresis loop, particularly during the upstroke phase [see Fig. 17(a)]. The same behavior is also observed for the reattachment point curves [see Fig. 17(b)]; specifically, in the upstroke phase at high angles of attack, a divergent trend is still apparent, albeit less pronounced than in the higher Reynolds number case.

A quantitative comparison between the results obtained by DIT at the two Reynolds numbers tested is provided in Figs. 18 and 19, showing, respectively, the direct comparison of the transition and reattachment points at the different reduced frequencies tested.

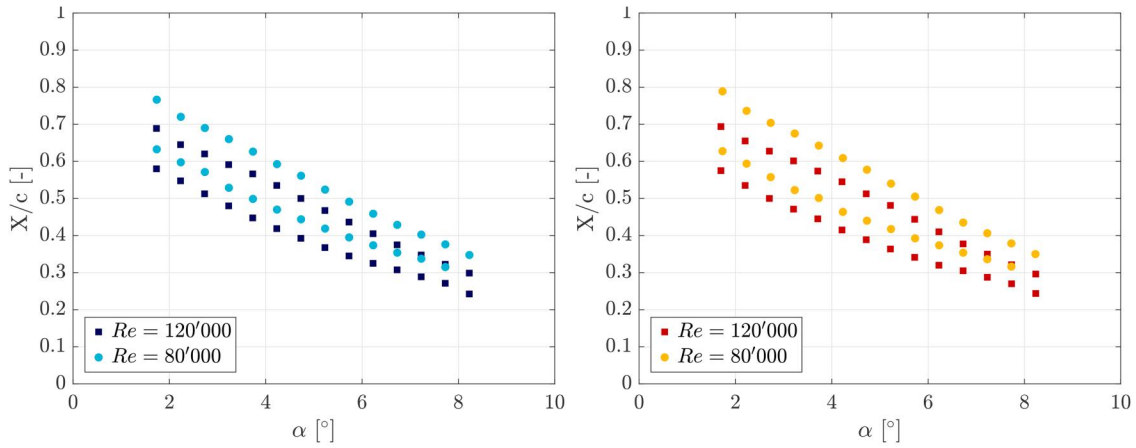

(a) $k = 0.0172$ (b) $k = 0.0343$

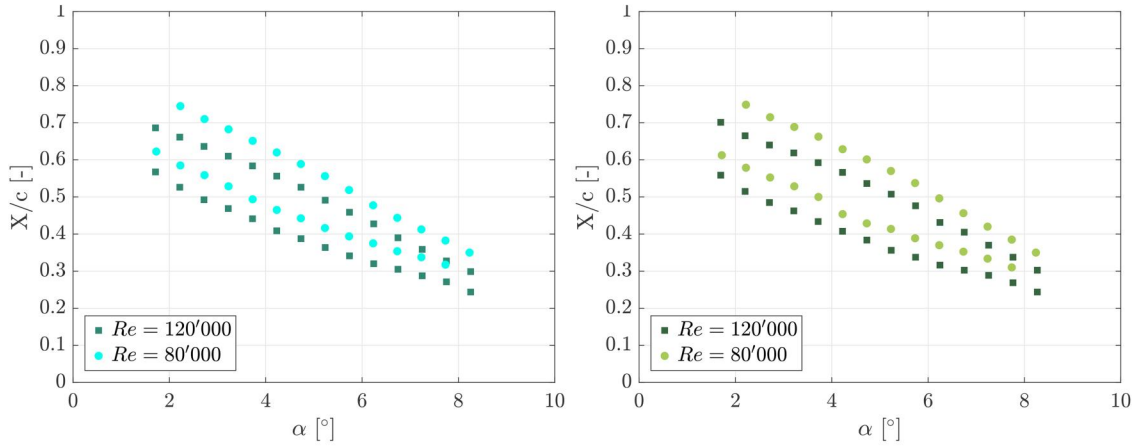

(c) $k = 0.0515$ (d) $k = 0.0687$

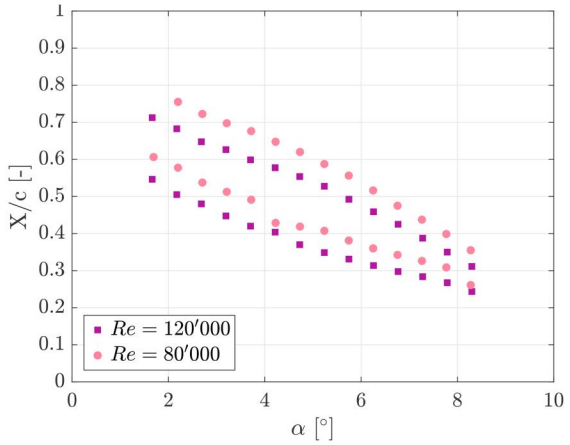

(e) $k = 0.1047$

FIG. 18. Comparison of the LSB transition point locations evaluated by DIT at different Reynolds numbers, $\bar{\alpha} = 5°$ and $\hat{\alpha} = 4°$.

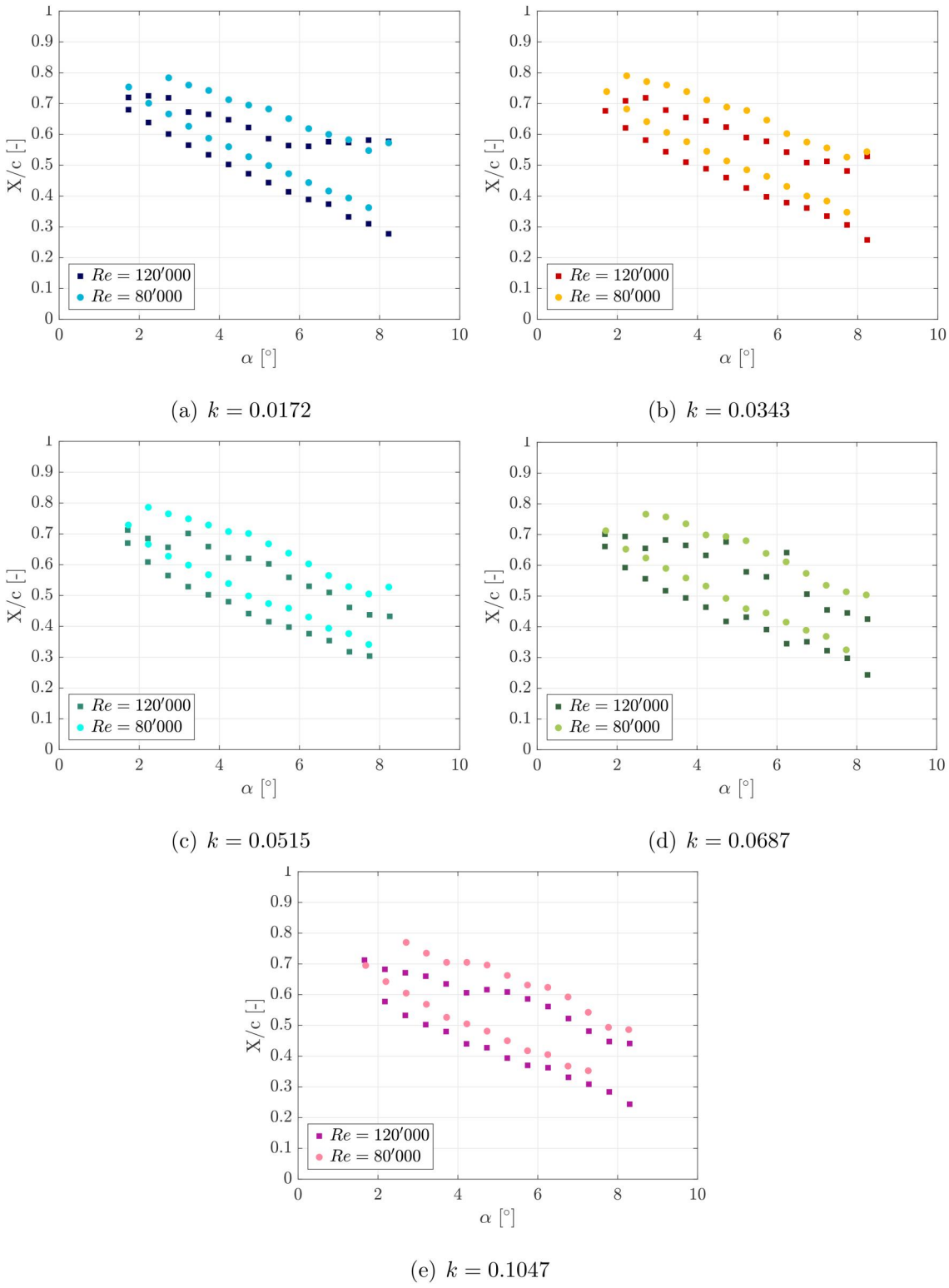

FIG. 19. Comparison of the LSB reattachment point locations evaluated by DIT at different Reynolds numbers, $\bar{\alpha} = 5^\circ$ and $\hat{\alpha} = 4^\circ$.

Figure 18 clearly shows that the transition point at the lower Reynolds number is positioned further downstream at all the reduced frequencies tested. In particular, the curves representing the transition point positions evaluated by DIT at the two different Reynolds numbers show an almost constant shift both in the upstroke and downstroke motions. This behavior is consistent with the results obtained in the present experiments under steady conditions. Indeed, as indicated by Wynnychuk and Yarusevych,[18] the Reynolds number acts as a fundamental driver for the onset of shear layer instability, where an increase in *Re* correlates with an accelerated spatial growth rate of Kelvin–Helmholtz instabilities within the separated shear layer. This mechanism promotes an upstream shift of the transition point, effectively shortening the streamwise extent of the laminar separation bubble (LSB).

Figure 19 shows that the Reynolds number effect observed during unsteady conditions at the transition point could also be extended to the reattachment point. In particular, during the downstroke motion, a similar upstream shift of the reattachment point position is observed for the higher Reynolds number. A similar effect is observed in the upstroke phase of the motion; however, at low reduced frequencies (i.e., $k = 0.0172$ and 0.0343), the comparison at high angles of attack highlights that the reattachment point at the lower *Re* moves upstream following a quite linear trend as expected, while a downstream divergence is observed only toward the highest angles of attack reached during the cycle. This behavior suggests that the divergent trend of the reattachment point in this area of the pitching motion could be correlated with shear layer instabilities promoted in a higher Reynolds number flow.

V. CONCLUSIONS

The present experimental investigation provided a comprehensive assessment of infrared thermography (IRT) and differential infrared thermography (DIT) as diagnostic tools for the characterization of laminar separation bubbles (LSBs) on a NACA 0018 airfoil. By exploring both steady and unsteady flow regimes at low Reynolds numbers, the study established a robust framework for tracking the dynamics of the LSB characteristic points. Specifically, it extended the knowledge regarding the reattachment point under sinusoidal pitching conditions and provided detailed insights into the effects of reduced frequency, oscillation amplitude, and Reynolds number on LSB positioning under periodic flow conditions.

In steady-state flow conditions, the surface temperature-based diagnostics were successfully validated through a comparative study against China Clay flow visualizations. The results confirmed that streamwise gradients of surface intensity reliably identify the separation (maximum gradient) and transition (minimum gradient) points. Among the evaluated criteria for reattachment point detection, the intersection point method demonstrated superior accuracy compared to the minimum intensity method, providing a more precise correlation with the physical reattachment observed in surface visualizations.

The application of the DIT technique to sinusoidal pitching cycles revealed a pronounced hysteresis in the LSB characteristics. Both transition and reattachment points exhibited significant spatial shifts between the upstroke and downstroke phases. The magnitude of this hysteresis was found to scale linearly with the pitching rate, indicating that the LSB dynamics are governed by the time-dependent lag of the boundary layer in adapting to the unsteady adverse pressure gradient.

In particular, the study highlighted that increasing the reduced frequency effectively strengthens the hysteresis loops of the investigated characteristic points. At high reduced frequencies, the boundary layer has insufficient time to equilibrate with the instantaneous angle of attack, leading to delayed transition and a more persistent separation bubble during the upstroke. On the other hand, at low reduced frequencies, a divergent trend in the reattachment point was observed at high angles of attack, possibly indicating the onset of shear layer instabilities or a breakdown of the LSB structure that traditional DIT sign-change criteria may struggle to capture.

The comparative analysis between the results obtained at $Re = 80\,000$ and $120\,000$ and confirmed that the Reynolds number remains a primary driver of LSB topology, even in unsteady conditions. An increase in *Re* consistently promoted an upstream shift of the transition and reattachment points, confirming the mechanisms outlined in steady flow conditions associated with the accelerated growth of flow instabilities within the separated shear layer. Indeed, the shift of the LSB characteristic point positions observed in unsteady regimes was found to be consistent with the trends established by measurements in static conditions.

This work confirms that differential infrared thermography is a mature and highly effective non-intrusive technique for investigating complex features such as separation bubbles under unsteady flow conditions. Generally, the findings provide a detailed, quantitative, and comprehensive database of LSB behavior on a pitching airfoil, extending the state of the art and highlighting the critical roles of pitching cycle parameters on the LSB characteristic points' locations. These results are of particular relevance for several unsteady applications at low Reynolds numbers, such as the optimization of micro air vehicles (MAVs), small-scale wind turbines, and unmanned systems operating in highly dynamic environments.

Although the present study focuses on relatively low oscillation amplitudes, larger amplitudes are expected to significantly alter the LSB dynamics. In particular, excursions toward higher angles of attack may promote instability or bursting of the separation bubble, weaken or suppress reattachment, and enhance shear layer instabilities leading to earlier transition. These effects would likely result in stronger unsteady behavior and more pronounced hysteresis, and could potentially introduce dynamic stall-like features even at low Reynolds numbers. A detailed investigation of these regimes is left for future work. In addition, further information such as pressure and skin friction distributions would provide complementary insight and could further enhance the characterization of the flow, particularly under unsteady conditions, and is therefore identified as a further direction for future work.

AUTHOR DECLARATIONS

Conflict of Interest

The authors have no conflicts to disclose.

Author Contributions

L. Riccobene: Conceptualization (lead); Investigation (equal); Methodology (lead); Resources (lead); Supervision (lead); Writing – original draft (equal); Writing – review & editing (equal). **M. Poletti:** Formal analysis (equal); Investigation (equal); Software (equal); Visualization (equal). **R. Tomasello:** Formal analysis (equal);

Investigation (equal); Software (equal); Visualization (equal). **A. Zanotti:** Conceptualization (equal); Supervision (equal); Writing – original draft (equal); Writing – review & editing (equal).

DATA AVAILABILITY

The data that support the findings of this study are available from the corresponding author upon reasonable request.

REFERENCES

[1]H. W. Stock, "Wind tunnel-flight correlation for laminar wings in adiabatic and heating flow conditions," Aerosp. Sci. Technol. **6**, 245–257 (2002).
[2]C. Purser, P. Marzocca, M. Marino, and D. Pook, "On the use of infrared thermography for boundary layer analysis," in *AIAA Scitech 2019 Forum* (AIAA, 2019).
[3]T. Astarita and G. M. Carlomagno, *Infrared Thermography for Thermo-Fluid-Dynamics* (Springer, Berlin Heidelberg, 2012).
[4]Y. Le Sant, M. Marchand, P. Millan, and J. Fontaine, "An overview of infrared thermography techniques used in large wind tunnels," Aerosp. Sci. Technol. **6**, 355–366 (2002).
[5]S. Zuccher and W. S. Saric, "Infrared thermography investigations in transitional supersonic boundary layers," Exp. Fluids **44**, 145–157 (2007).
[6]T. Astarita and G. M. Carlomagno, "Infrared thermography for thermo-fluid-dynamics," in *Experimental Fluid Mechanics*, 1st ed. (Springer, Berlin, Heidelberg, 2012).
[7]L. de Luca, G. M. Carlomagno, and G. Buresti, "Boundary layer diagnostics by means of an infrared scanning radiometer," Exp. Fluids **9**, 121–128 (1990).
[8]M. Raffel and C. B. Merz, "Differential infrared thermography for unsteady boundary-layer transition measurements," AIAA J. **52**, 2090–2093 (2014).
[9]A. D. Gardner, C. Eder, C. C. Wolf, and M. Raffel, "Analysis of differential infrared thermography for boundary layer transition detection," Exp. Fluids **58**, 1–14 (2017).
[10]C. C. Wolf, C. Mertens, A. D. Gardner, C. Dollinger, and A. Fischer, "Optimization of differential infrared thermography for unsteady boundary layer transition measurement," Exp. Fluids **60**(1), 13 (2019).
[11]M. Raffel, C. B. Merz, T. Schwermer, and K. Richter, "Differential infrared thermography for boundary layer transition detection on pitching rotor blade models," Exp. Fluids **56**, 1–13 (2015).
[12]A. D. Gardner, C. C. Wolf, J. T. Heineck, M. Barnett, and M. Raffel, "Helicopter rotor boundary layer transition measurement in forward flight using an infrared camera," J. Am. Helicopter Soc. **65**, 2–14 (2020).
[13]C. C. Wolf, A. D. Gardner, and M. Raffel, "Infrared thermography for boundary layer transition measurements," Meas. Sci. Technol. **31**, 112002 (2020).
[14]G. M. Cole and T. J. Mueller, "Experimental measurements of the laminar separation bubble on an Eppler 387 airfoil at low Reynolds numbers," NASA Technical Report No. UNDAS-1419-FR (NASA, 1990).
[15]E. Gartenberg, A. Roberts, and G. McRee, "Infrared imaging and tufts studies of boundary layer flow regimes on a NACA 0012 airfoil," in *International Congress on Instrumentation in Aerospace Simulation Facilities* (IEEE, 1989), pp. 168–178.
[16]S. Montelpare and R. Ricci, "A thermographic method to evaluate the local boundary layer separation phenomena on aerodynamic bodies operating at low Reynolds number," Int. J. Therm. Sci. **43**, 315–329 (2004).
[17]R. Ricci, S. Montelpare, and E. Renzi, "Study of mechanical disturbances effects on the laminar separation bubble by means of infrared thermography," Int. J. Therm. Sci. **50**, 2091–2103 (2011).
[18]D. W. Wynnychuk and S. Yarusevych, "Characterization of laminar separation bubbles using infrared thermography," AIAA J. **58**, 2831–2843 (2020).
[19]A. Grille Guerra, C. Mertens, J. Little, and B. van Oudheusden, "Experimental characterization of an unsteady laminar separation bubble on a pitching wing," Exp. Fluids **64**(1), 19 (2023).
[20]R. Tomasello, "Infrared thermography investigation of boundary layer transition on an airfoil model," Master's thesis (Politecnico di Milano, 2024).
[21]M. Poletti, "Experimental characterization of an unsteady laminar separation bubble on a pitching airfoil by infrared thermography," Master's thesis (Politecnico di Milano, 2025).
[22]A. D. Gardner, C. C. Wolf, and M. Raffel, "A new method of dynamic and static stall detection using infrared thermography," Exp. Fluids **57**, 1–13 (2016).
[23]M. Costantini, U. Fey, U. Henne, and C. Klein, "Influence of non-adiabatic model surface on transition measurements using the temperature-sensitive paint technique in a cryogenic wind tunnel," in *42nd AIAA Fluid Dynamics Conference and Exhibit* (AIAA, 2012).
[24]W. Lang, A. D. Gardner, S. Mariappan, C. Klein, and M. Raffel, "Boundary-layer transition on a rotor blade measured by temperature-sensitive paint, thermal imaging and image derotation," Exp. Fluids **56**, 1–14 (2015).
[25]A. Weiss, A. D. Gardner, C. Klein, and M. Raffel, "Boundary-layer transition measurements on Mach-scaled helicopter rotor blades in climb," CEAS Aeronaut. J. **8**, 613–623 (2017).
[26]J. G. Leishman, *Principles of Helicopter Aerodynamics* (Cambridge University Press, 2006).
[27]A. Zanotti and G. Gibertini, "Experimental investigation of the dynamic stall phenomenon on a NACA 23012 oscillating airfoil," Proc. Inst. Mech. Eng., Part G **227**, 1375–1388 (2013).
[28]T. Theodorsen, "General theory of aerodynamic instability and the mechanism of flutter," NACA Technical Report No. NACA-TR-496 (NACA, 1935).
[29]K. Richter, C. C. Wolf, A. D. Gardner, and C. B. Merz, "Detection of unsteady boundary layer transition using three experimental methods," in *54th AIAA Aerospace Sciences Meeting* (AIAA, 2016).
[30]A. D. Gardner, C. B. Merz, and C. C. Wolf, "Effect of sweep on a pitching finite wing," J. Am. Helicopter Soc. **64**, 1–13 (2019).
[31]A. Weiss, C. Klein, U. Henne, and A. Hebler, "Unsteady boundary-layer transition measurements with temperature-sensitive paint under cryogenic conditions," Exp. Therm. Fluid Sci. **163**, 111414 (2025).